Thermal analysis of selected tin-based lead-free solder alloys

M. Palcut[1,4], J. Sopoušek[2]*, L. Trnková[1], E. Hodúlová[3], B. Szewczyková[3], M. Ožvold[1],
M. Turňa[3], J. Janovec[1]

[1]*Institute of Materials Science, Faculty of Material Science and Technology, Slovak University of Technology,
917 24 Trnava, Slovak Republic*
[2]*Institute of Chemistry, Faculty of Science, Masaryk University, 611 37 Brno, Czech Republic*
[3]*Institute of Production Technologies, Faculty of Material Science and Technology, Slovak University of Technology,
917 24 Trnava, Slovak Republic*
[4]*Division of Fuel Cells and Solid State Chemistry, Risø National Laboratory, Technical University of Denmark,
4000 Roskilde, Denmark*

Abstract

The Sn-Ag-Cu alloys have favourable solderability and wetting properties and are, there-fore, being considered as potential lead-free solder materials. In the present study, tin-based Sn-Ag-Cu and Sn-Ag-Cu-Bi alloys were studied in detail by a differential scanning calorimetry (DSC) and thermodynamic calculations using the CALPHAD approach. The amount of the alloying elements in the materials was chosen to be close to the respective eutectic composition and the nominal compositions were the following: Sn-3.7Ag-0.7Cu, Sn-1.0Ag-0.5Cu-1Bi (in wt.%). Thermal effects during melting and solidifying were experimentally studied by the DSC technique. The microstructure of the samples was determined by the light microscopy and the composition of solidified phases was obtained by the energy-dispersive X-ray spectro-scopy, respectively. The solidification behaviour under equilibrium conditions was simulated using the Thermo-Calc software package. This approach enabled us to obtain the enthalpy of cooling for each alloy and to compare its temperature derivative with the experimental DSC curves.

K e y w o r d s: lead-free solders, DSC, CALPHAD, phase equilibria

1. Introduction

Due to the restrictions posed on the use of lead in industry, the lead-free solders have received a consider-able attention over the years. Among several potential candidate systems investigated, tin-rich Sn-Ag-Cu al-loys have been found to be one of the most promising alternatives. These alloys have favourable solderabil-ity, mechanical and wetting properties [1–3]. In the soldering process, three consecutive steps are import-ant: a) melting of the solder alloy, b) contacting and solidifying of the alloy on the metal substrate and c) the ageing of the solder joint during solidification [4]. The melting and solidification behaviour as well as the interfacial reactions taking place during operation all influence the performance and durability of the solder joint. Since the alloy systems often solidify in the eu-tectic composition, the location of the eutectic point is of primary importance.

The ternary eutectic of the Sn-Ag-Cu alloy is known to be present in the tin-rich corner of the tern-ary system [5]. The ternary eutectic has been found to melt at temperatures close to 217 °C and the compos-ition was determined to be 4.7 wt.% Ag and 1.7 wt.% Cu by Miller et al. [6] and 3.5 wt.% Ag and 0.9 wt.% Cu by Loomans and Fine [7].

Ohnuma et al. did an important work in the ther-modynamic assessment of the Sn-Ag-Cu system. They used a database consisting of 8 metals (Pb, Bi, Sn, Sb, Cu, Ag, Zn, and In) [8]. The authors identified the following eutectic reaction at 3.24 wt.% Ag and 0.57 wt.% Cu and 217.7 °C:

$$\text{Liquid} \rightarrow (\beta\text{Sn}) + \text{Cu}_6\text{Sn}_5 + \text{Ag}_3\text{Sn}, \qquad (1)$$

and presented the phase fraction change of the ternary eutectic alloy during solidification. The solidification process has also been studied in detail [8] under the equilibrium and non-equilibrium conditions using the Scheil module of Thermo-Calc. The authors found that the solidification starts with the primary crystals of (βSn) and is terminated when it reaches the ternary eutectic reaction at 217.7 ℃. They found the difference between the Scheil mode and the equilibrium solidification was relatively small.

The melting temperature of the Pb-Sn eutectic solder alloy is only 183 ℃. The possibility of decreasing the melting temperature of the Sn-Ag-Cu alloy has been, therefore, investigated using additional elements such as Bi or In. It has been proposed by Ohnuma et al., that the melting temperature should decrease and the solidification range should increase with increasing Bi and In content in line with the following reactions [8]:

$$\text{Liquid} \rightarrow (\beta\text{Sn}) + \text{Cu}_6\text{Sn}_5 + \text{Ag}_3\text{Sn} + \text{liquid} \qquad (2)$$
$$\text{for } 0 \leq \text{wt.\% Bi} \leq 12 \text{ or } 0 \leq \text{wt.\% In} \leq 1.9,$$

$$\text{Liquid} \rightarrow (\beta\text{Sn}) + \text{Cu}_6\text{Sn}_5 + (\zeta\text{Ag}) + \text{liquid} \qquad (3)$$
$$\text{for } 1.9 \leq \text{wt.\% In} \leq 7.1,$$

$$\text{Liquid} \rightarrow (\gamma\text{Sn}) + \text{Cu}_6\text{Sn}_5 + (\zeta\text{Ag}) + \text{liquid} \qquad (4)$$
$$\text{for } 7.1 \leq \text{wt.\% In} \leq 12.$$
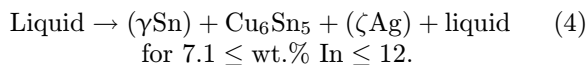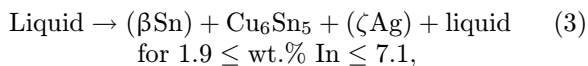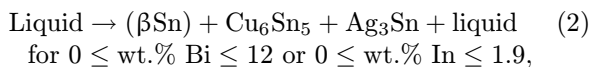
The content of silver and copper in the eutectic melt was proposed to change depending on the content of Bi and In. This indicates that the relationship between the melting temperature and composition of the alloy should be maintained for efficient alloy design. The solidification simulation using the Scheil module of Sn-2.0Ag-0.5Cu-7.5Bi alloy showed that the solidification started with the primary crystals of Cu_6Sn_5 [8]. It proceeded substantially, with the growth of (βSn) at the beginning. After commencement of the crystallization of Ag_3Sn phase, the liquid would disappear at 177.9 ℃ under the equilibrium solidification condition. Nevertheless, according to the Scheil model, the Bi is concentrated in the liquid phase during solidification, which causes an extensive fall of terminating temperature of solidification. The final temperature, 139.9 ℃, corresponds to the eutectic temperature of the Sn-Bi binary alloy [8]. The behaviour of such a residual liquid phase at low temperatures is considered to cause a lifting-off failure at the interface between the solder and the Cu substrate.

In the present work, two tin-based alloys Sn-Ag--Cu and Sn-Ag-Cu-Bi with compositions close to the respective eutectic composition were studied in detail. The thermal effects during melting and solidifying were investigated by differential scanning calorimetry

(DSC) in an inert atmosphere by changing the heating and cooling rates. The microstructure of the samples and the composition of solidified phases were determined by the scanning electron microscopy and energy dispersive spectroscopy. The solidification behaviour was also considered using the Scheil-Gulliver model [9, 10].

2. Experimental

2.1. The sample preparation

The samples were prepared by a controlled melting of pure Sn, Ag, Cu, and Bi in the respective concentrations in alumina crucibles. An inductive heating of the metal elements was applied. The melt was stirred constantly. The melted alloys were quenched in air by pouring the content of the crucible on a piece of cold steel plate. The chemical compositions of the samples were Sn-3.7wt.%Ag-0.7wt.%Cu (sample S1, Sn-3.7Ag-0.7Cu) and Sn-1.0wt.%Ag-0.5wt.%Cu--1.0wt.%Bi (sample S2, Sn-1Ag-0.5Cu-1Bi).

2.2. Microscopy/EDX

For the microscopy characterisation, the samples were mounted in epoxy resin and polished using a diamond abrasive (1 micrometer finish). Both the light and scanning electron microscopy were employed. Alloy phases were identified and analysed using the scanning electron microscope (SEM) JEOL 6460 equipped by the energy dispersive microanalyser (EDS) INCA Energy.

2.3. Thermal analysis

The thermal analysis was carried out using the Netzsch STA 409 CD/3/403/5/G Apparatus. This instrument enables a detection of the differential scanning calorimetry signal (heat flow DSC) and allows for the measurements in the temperature range of 25–1400 ℃ with heating and cooling rates of 0.1–20 K min^{-1}. The thermal effect upon heating and cooling was measured on the samples at several different heating and cooling rates. The first thermal cycle was started with a rate of 10 K min^{-1}. Each subsequent cycle was carried out at a lower heating and cooling rate with respect to the previous cycle, with heating and cooling rates going down to 0.1 K min^{-1}. The time to sensitivity optimal heating and cooling rate for the samples S1 and S2 were found to be 1 K min^{-1} since it allowed for the sufficient separation of peak minima. The experiments were all carried out in an inert gas atmosphere using a constant flow of argon (70 ml min^{-1}). All measurements were referenced to an empty crucible.
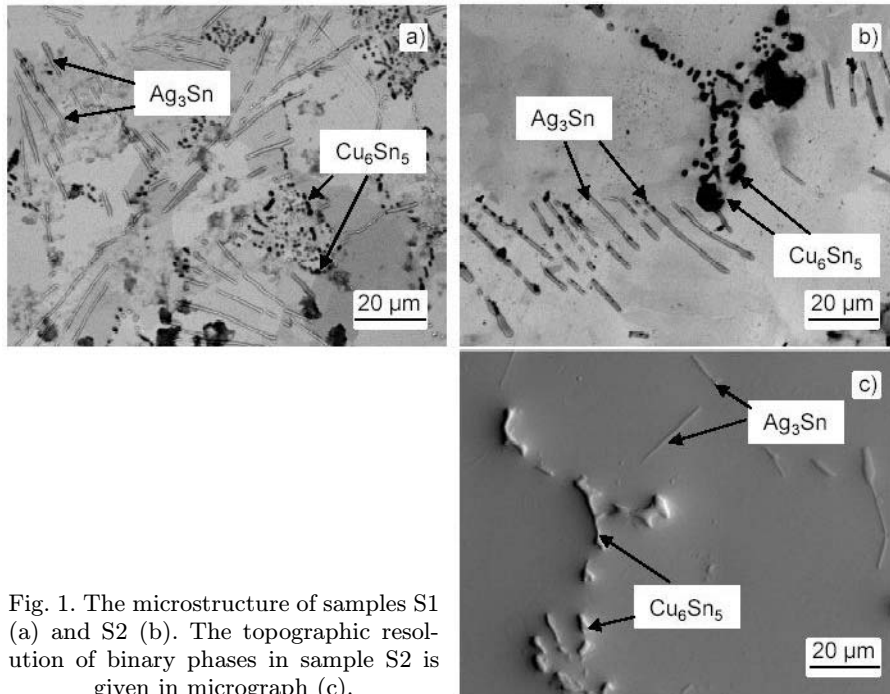
Fig. 1. The microstructure of samples S1 (a) and S2 (b). The topographic resolution of binary phases in sample S2 is given in micrograph (c).

T a b l e 1. Bulk compositions measured by EDX and experimental chemical compositions (in wt.%) of the matrix and secondary phases of samples S1 and S2. Theoretical compositions: matrix close to 100 wt.% Sn, Ag_3Sn – 26.8 wt.% Sn, Cu_6Sn_5 – 60.9 wt.% Sn

	S1				S2			
	Bulk	Matrix	Ag_3Sn	Cu_6Sn_5	Bulk	Matrix	Ag_3Sn	Cu_6Sn_5
Sn	95.6	99.7	23.8	63.4	97.5	98.3	28.5	63.7
Ag	3.7	0.0	75.7	0.5	1.0	0.1	71.0	0.4
Cu	0.7	0.3	0.5	36.1	0.5	0.3	0.4	35.5
Bi	–	–	–	–	1.0	1.3	0.1	0.3

3. Results

3.1. Electron microscopy

The SEM micrographs of the quenched samples are given in Fig. 1. The micrographs are shown in the backscatter mode to provide the element contrast. The structure of all samples consisted of the matrix and binary phases precipitated during solidification. The chemical composition of the samples is given in Table 1. The amount of precipitated phases corresponded to the element weight fraction of Cu and Ag in each alloy. The amount of precipitated Ag_3Sn phase was higher in the sample 1 (S1) since the sample 1 had higher silver content (Table 1). The amount of the Cu_6Sn_5 phase was roughly the same in all alloys since the copper content in all samples was very similar. The Ag_3Sn phase formed lamellas whilst the Cu_6Sn_5 phase formed round shape particles in the samples 1 and 2.

The chemical composition of the precipitated phases is given in Table 1. The results for the secondary phases were obtained by the spot microanalysis mode of the energy dispersive X-ray spectroscopy. The matrix consisted mostly of Sn and the composition of phases Ag_3Sn and Cu_6Sn_5 was close to the respective stoichiometric compositions. The composition of the matrix and of the precipitated phases remained almost unchanged by the presence of bismuth.

The distribution of binary phases in the samples may reveal the mechanism of crystallisation. It can be suggested that the precipitation of binary phases in sample S2 started at separated nucleation centres. Secondary phases in S2, especially the Cu_6Sn_5, were located mostly along grain boundaries. This location suggests that these phases started to precipitate later than the matrix. The location of the Cu_6Sn_5 phase at grain boundaries and triple junctions suggests that this phase started to precipitate earlier than Ag_3Sn.
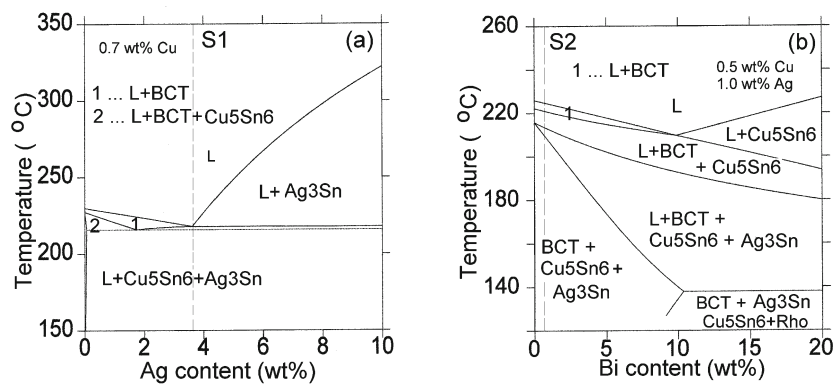
Fig. 2. Calculated phase diagram cross-sections of the Sn-Ag-Cu ((a) – left) and Sn-Ag-Cu-Bi ((b) – right) systems. Dashed lines represent the composition of alloys S1 and S2.
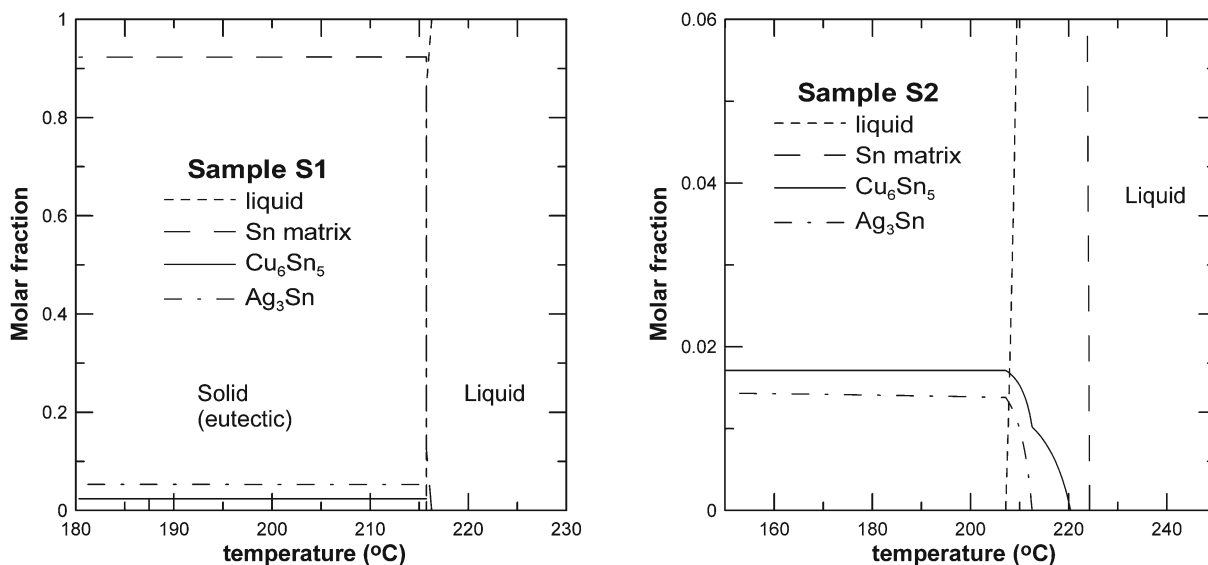
Fig. 3. Calculated equilibrium molar fractions of the phases in alloys Sn-3.7Ag-0.7Cu ((a) – left) and Sn-1Ag-0.5Cu-1Bi ((b) – right).

3.2. Thermodynamic calculations

The thermodynamic modelling employed the CAL-PHAD approach [11]. The equilibrium calculations were performed using the Thermo-Calc software package [12]. The individual phases and their molar Gibbs energies were described by the parameters taken from the COST531 Thermodynamic Database of Lead-free Solders, version 2.0b, which was used in all our calculations [13, 14]. This database contains critically assessed thermodynamic data for eleven elements (Ag, Au, Bi, Cu, In, Ni, Pb, Pd, Sb, Sn, Zn) and for the most binary and ternary systems consisting of these elements. On the link [15] you can get more details on the database. The calculated phase diagrams are available in [16].

The tin-rich section of the phase diagram of the Sn-Ag-Cu system, with a constant copper content of $w(\mathrm{Cu}) = 0.7$ %, is given in Fig. 2a. The phases present

in the system are the following: liquid (L), the solid solution of silver in βSn (BCT), $\mathrm{Ag_3Sn}$ and $\mathrm{Cu_6Sn_5}$. The experimental composition of the alloy, given by the dashed line, is very close to the eutectic composition. This allows for the parallel precipitation of all phases, in line with our observations (Fig. 1a). The tin-rich section of the phase diagram of the Sn-Ag-Cu-Bi system, with constant copper and silver contents of $w(\mathrm{Cu}) = 0.5$ % and $w(\mathrm{Ag}) = 1.0$ %, is given in Fig. 2b. The phases present in this system are the following: liquid (L), the solid solution of silver in βSn (BCT), $\mathrm{Ag_3Sn}$, and $\mathrm{Cu_6Sn_5}$. In addition to system S1, there is a rhombohedral phase of the solid solution of Bi in Sn (Rho). The dashed line represents the composition of the sample S2. The point when the last liquid disappears is predicted to be close to 140 °C, if the bismuth content is over 10 wt.%. But this is not the case of sample S2, having 1 wt.% of Bi only.

The calculated equilibrium molar fractions of the

phases for systems S1 and S2 are given in Fig. 3. The precipitation of all phases in sample S1 is predicted to happen in parallel and at temperature of about 217℃ (Fig. 3a). This temperature is close to the temperature reported for the ternary eutectic of the Sn-Ag-Cu system. The precipitation in the Sn-1.0Ag-0.5Cu-1Bi alloy is more complicated and starts probably with the tin matrix and continues with the secondary phases. The Cu_6Sn_5 phase is predicted to start precipitating earlier than the Ag_3Sn phase. Since the precipitation of the phases in the system S2 does not happen at the same temperature, one may expect several signals in the DSC curve.

3.3. DSC curve simulations

An important source of information about the phase transformations provides the heat-flux differential scanning microscopy (DSC). It represents the heat flux signals of the sample upon heating and cooling. The heat flux of the sample upon cooling should, in a perfect state, copy the heating signal. The cooling, however, is often influenced by a supercooling effect, which makes the signal less reliable. The heating signal has been, therefore, used in the present study to gain further information about the phase transformations of the lead-free solder materials.

The DSC signal of sample S1 is given in Fig. 4. The heating curve consists of one minimum, which reflects the heat flux upon melting of the alloy in the eutectic composition. The DSC signal of sample S2, given in Fig. 5, is more complicated. It consists, depending on the heating rate, of one broad peak or of a superposition of three peaks. The peak parameters
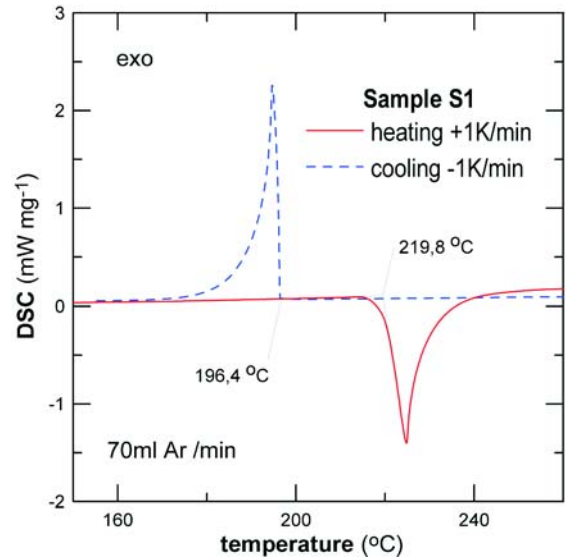
Fig. 4. Experimental DSC heating (red) and cooling (blue) curves of sample S1. Heating and cooling rates were 1 K min^{-1}.

of samples S1 and S2 at the heating rate of 1 K min^{-1} are represented in Table 2.

Since the CALPHAD approach allows for the calculation of thermodynamic functions, the DSC curves could be simulated using the calculated molar enthalpies of the solder alloys, ΔH. The temperature dependences of the standard molar enthalpies of the samples S1 and S2 are presented in Fig. 6. The molar enthalpies were referenced to the standard element reference state (SER, temperature 25℃, pressure 1 at).
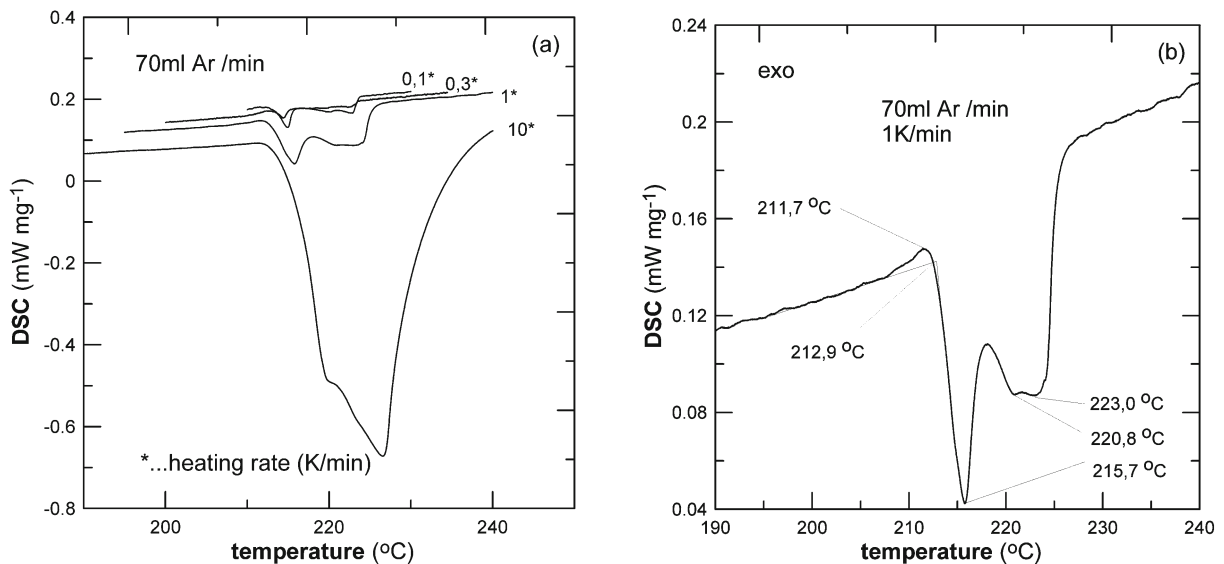
Fig. 5. Experimental DSC heating curves of sample S2 of different heating rates ((a) – left) and detail for the heating rate 1 K min^{-1} ((b) – right)

Table 2. The experimental and predicted peak positions (in ℃) in the DSC heating curves of samples S1 and S2 at heating rate 1 K min^{-1}

		Experiment		Theory	
S1 (Sn-3.7Ag-0.7Cu)	Start	215.9	Eutectic temp.	216. 7
	Minimum	234	No meaning	–
S2 (Sn-1.0Ag-0.5Cu-1Bi)	Start	211.7	Start of melting	207.6
	1st minimum	215.7	Ag$_3$Sn dissolution	213.6
	2nd minimum	220.8	Cu$_6$Sn$_5$ dissolution	221.1
	3rd minimum	223.0	Sample melting	224.0
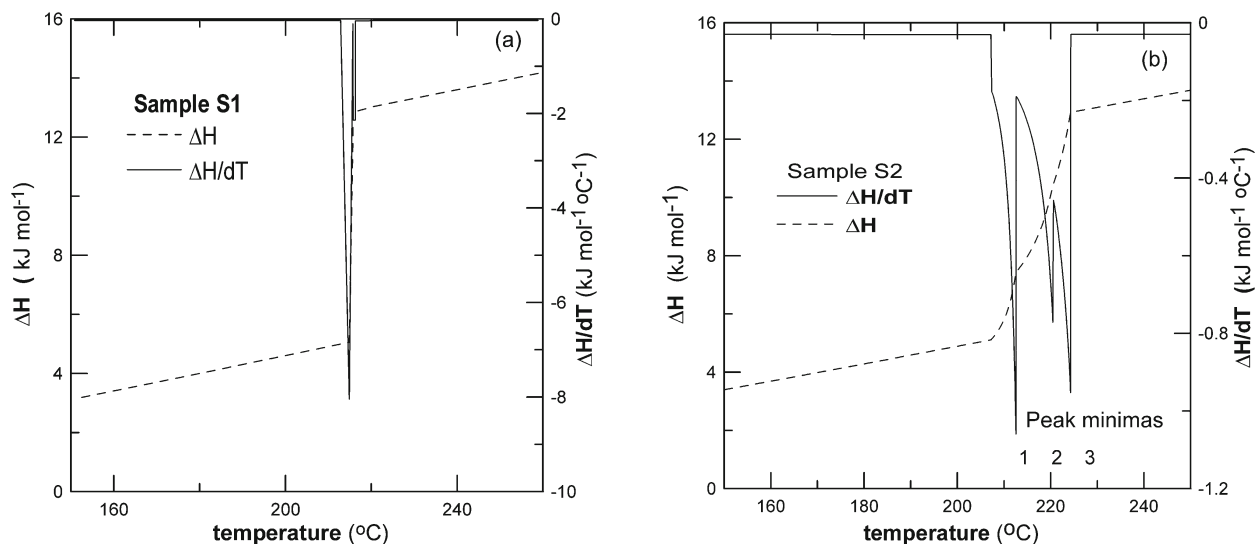
Fig. 6. Calculated molar enthalpies of the alloys Sn-3.7Ag-0.7Cu ((a) – left) and Sn-1.0Ag-0.5Cu-1Bi ((b) – right) and the respective numerical temperature derivations at different temperatures.

The molar enthalpy of alloy S1 has a simple "step--like" shape with narrow transition region corresponding to the melting of the eutectic alloy at 215–216 ℃ (Fig. 6a). The enthalpy change upon heating from 215 to 216 ℃ corresponds to the latent heat of melting of the eutectic composition. The temperature dependence of the molar enthalpy of alloy S2 is more complicated. It exhibits a broad transition region between the fully solid and fully liquid states (Fig. 6b). Its shape is given by the phase transitions, in line with the phase diagram given in Fig. 2.

The temperature derivative of the molar enthalpy corresponds to the heat capacity. Since the experimental DSC signal corresponds to the enthalpy changes with respect to the temperature, the numerical temperature derivative of the molar enthalpy corresponds to the DSC curve, too. The temperature derivative of the molar enthalpy of the alloy S1 has one sharp minimum (Fig. 6a). The temperature derivative of the molar enthalpy of alloy S2 has three minima. The peak positions are given in Fig. 6b and Table 2.

4. Discussion

The CALPHAD method and the thermodynamic database COST 531 of lead-free solders alloys have been used to predict the phase transformations in the Sn-3.7Ag-0.7Cu, Sn-1.0Ag-0.5Cu-1Bi systems. The matrix, formed mainly by the βSn, and two binary phases, Cu$_6$Sn$_5$ and Ag$_3$Sn, form the composition of the solidified samples. The calculated and experimental element compositions of the phases were nearly identical (Table 1). The agreement between the experimental and calculated results shows that the chosen thermodynamic database contains reliable data, which can be used for the consequent study of the investigated systems.

The interpretation of the experimental curves was based on the CALPHAD approach and utilized the procedure introduced by Boettinger et al. [17, 18]. They showed that the experimental DSC curve might be simulated using the temperature derivative of molar enthalpy and by introducing the technical parameters of the equipment.

The interpretation of the experimental DSC curves using the CALPHAD approach requires the thermodynamic equilibrium to be established in the samples. This can be achieved only by decreasing the heating and cooling rates, ideally approaching the values close to $0\,K\,min^{-1}$. The role of the heating and cooling rates on the DSC signals has been demonstrated (see Fig. 5a). Lowering the heating rate allowed for a better peak deconvolution. The technical parameters of the equipment could be neglected. Since the agreement between the experimental data and thermodynamic predictions was very good, we can conclude that the heating rate of $1\,K\,min^{-1}$ was sufficient to achieve the thermodynamic equilibrium in the tin-based alloys near the respective eutectic temperature. The non-equilibrium Scheil-Gulliver model did not provide better results than the CALPHAD approach. The lack of agreement between the non-equilibrium solidification model and the experimental DSC curves is also showing that the thermodynamic equilibrium was achieved in the samples during the DSC measurements by using considerably low heating rates.

5. Conclusion

In the present work, we have provided the experimental phase compositions as well as the theoretical predictions of the phase transformations of solidified lead-free solder materials Sn-3.7Ag-0.7Cu and Sn-1.0Ag-0.5Cu-1Bi. The thermodynamic calculations employed the CALPHAD approach. The individual phases and their molar Gibbs energies were described by the parameters of the COST531 Thermodynamic Database of Lead-free Solders. The thermal effects during melting and solidification were investigated using the heat-flow differential scanning calorimetry. The theoretical DSC signals were simulated using the calculated molar enthalpies and their numerical temperature derivatives.

The chosen database proved to be reliable since the experimental and predicted phase compositions of the samples were close to identical. The interpretation of the experimental DSC curves based on the CALPHAD approach is a reliable method for testing the consistency between the phase diagrams and DSC signals. The heating and cooling rate of $1\,K\,min^{-1}$, used in most of the DSC measurements, was probably sufficient to achieve the state close to thermodynamic equilibrium in investigated materials. Since the numerical temperature derivative of calculated molar enthalpies was sufficient and provided the quantitative agreement between the experimental and simulated DSC curves, the technical parameters of the DSC equipment did not need to be taken into account. The omission of the equipment parameters leads to a substantial simplification of the theoretical model for the DSC curve simulation presented by Boettinger et al. [17, 18] and makes it more accessible by average user.

References

[1] SUGANUMA, K: Current Opinion in Solid State and Materials Science, 5, 2001, p. 55.
[2] KISIEL, R.—GASIOR, W.—MOSER, Z.—PSTRUS, J.—BUKAT, K.—SITEK, J.: Archives of Metallurgy and Materials, 50, 2005, p. 1065.
[3] GASIOR, W.—MOSER, Z.—DEBSKI, A.: Archives of Metallurgy and Materials, 49, 2004, p. 575.
[4] IPSER, H.—FLANDORFER, H.—LUEF, C.—SCHMETTERER, C.—SAED, U.: Journal of Materials Science – Materials in Electronics, 18, 2007, p. 3.
[5] MOON, K.-W.—BOETTINGER, W. J.—KATTNER, U. R.—BIANCANIELLO, F. S.—HANDWERKER, C. A.: Journal of Electronic Materials, 29, 2000, p. 1122.
[6] MILLER, C. M.—ANDERSON, I. E.—SMITH, J. F.: Journal of Electronic Materials, 23, 1994, p. 595.
[7] LOOMANS, M. E.—FINE, M. E.: Metallurgical and Materials Transactions A – Physical Metallurgy and Materials Science, 31, 2000, p. 1155.
[8] OHNUMA, I.—MIYASHITA, M.—ANZAI, K.—LIU, X. J.—OHTANI, H.—KAINUMA, R.—ISHIDA, K.: Journal of Electronic Materials, 29, 2000, p. 1137.
[9] GULLIVER, C. H.: Journal Institute of Metals, 9, 1913, p. 120.
[10] SCHEIL, E.: Zeitschrift für Metallkunde, 34, 1942, p. 70.
[11] SAUNDERS, N.—MIODOVNIK, A. P.: CALPHAD (calculation of phase diagram) – A Comprehensive Guide. Amsterdam, Elsevier Science 1998.
[12] ANDERSSON, J.-O.—HELANDER, T.—HÖGLUND, L.—SHI, P.—SUNDMAN, B.: Calphad, 26, 2002, p. 273.
[13] KROUPA, A.—VÍZDAL, J.: Defect and Diffusion Forum, 263, 2007, p. 99.
[14] KROUPA, A.— DINSDALE, A. T.—WATSON, A.—VŘEŠŤÁL, J.—VÍZDAL, J.— ZEMANOVÁ, A.: JOM, 59, 2007, p. 20.
[15] Database SOLDER at http://www.slihot.co.uk/COST531/td_database.htm.
[16] DINSDALE, A. T.—WATSON, A.—KROUPA, A.—VŘEŠŤÁL, J.—ZEMANOVÁ, A.—VÍZDAL, J.: COST Action 531 – Atlas of Lead-free Soldering. COST Office 2008, ISBN 978-80-86292-28-1.

[17] BOETTINGER, W. J.—KATTNER, U. R.: Metallurgical and Materials Transactions A – Physical Metallurgy and Materials Science, 33, 2002, p. 1779.

[18] BOETTINGER, W. J.—KATTNER, U. R.—MOON, K.-W.—PEREPEZKO, J. H.: DTA and Heat-flux DSC Measurements of Alloy Melting and Freezing. Washington, National Institute of Standards and Technology 2006.